



Suppressed recombination of electrons and holes and its role on the improvement of photoreactivity of flame-synthesized TiO₂ nanopowders

HyunSeock Jie^a, Hoon Park^a, Keun-Hwa Chae^b, Masakazu Anpo^c, Jong-Ku Park^{a,*}

^aNano-Science Research Division, Korea Institute of Science and Technology, Cheongryang, P.O. Box 131, Seoul 130-650, Republic of Korea

^bMaterials Science and Technology Research Division, Korea Institute of Science and Technology, Cheongryang, P.O. Box 131, Seoul 130-650, Republic of Korea

^cDepartment of Applied Chemistry, Graduate School of Engineering, Osaka Prefecture University, 1-1 Gakuen-cho, Sakai Osaka, Japan

ARTICLE INFO

Article history:

Received 28 October 2008

In final form 20 January 2009

Available online 29 January 2009

ABSTRACT

An in-situ NEXAFS study was performed to directly investigate the change in the hole structures in the conduction band of TiO₂ nanopowders synthesized using a flame method under UV irradiation. The anatase/rutile phase boundary was found to suppress the hole–electron recombination, leading to improved photoreactivity of TiO₂ nanopowders.

© 2009 Elsevier B.V. All rights reserved.

1. Introduction

Titanium oxide (TiO₂) nanopowders with photocatalytic properties have been fabricated using various methods, including sol-gel, hydrothermal treatment, and other physical methods [1–3]. Among these methods, the flame synthesis approach is one of the most popular methods for preparing TiO₂ nanopowders with high photocatalytic performance [4–6]. In general, the flame synthesis of TiO₂ nanopowders is carried out at high temperature above 900 °C, affording TiO₂ nanoparticles with very high degrees of crystallinity. Therefore, no additional calcination at high temperature is necessary to improve the crystallinity [7–12]. This fabrication method results in a low degree of agglomeration of the TiO₂ nanoparticles, which is crucial to obtaining high dispersivity in liquid media as well as a large specific surface area. Although TiO₂ nanopowders with an anatase structure have peculiar characteristics applicable to the various fields related to photo-induced electrons, many studies have sought to improve the photoreactivity of TiO₂ nanopowders and to expand the light harvesting range to visible light. The characteristics of TiO₂ nanopowders are known to sensitively depend on the synthesis method used. Each method has its own advantages and limitations with respect to controlling the properties of the TiO₂ nanopowders. The properties of a synthesized TiO₂ nanopowder can, however, be altered by post-treatments such as surface treatment in acid solution [13] and heat treatment at elevated temperature in a controlled atmosphere [4,14].

Of course, the effects of such post-treatments on the properties of a TiO₂ nanopowder cannot be completely separated from the synthesis method used to produce the nanopowder, because the

lattice defects inside the particles, and the anatase-to-rutile phase ratios, are determined by the process conditions as well as by the method of synthesis.

Here we present the results of a direct investigation of the hole structures in the conduction band of flame-synthesized TiO₂ nanopowders that have been subsequently heat-treated at various temperatures. In addition, we examine the possible link between changes in the hole structures determined directly under UV irradiation, and the photocatalytic performance of the respective TiO₂ nanopowders.

2. Experimental

2.1. Preparation of photocatalysts

The TiO₂ nanopowders were synthesized by a flame method using titanium tetra-isopropoxide (TTIP-Aldrich, 97%) as a precursor. The TTIP vapour was vaporized in an oil bath and delivered to the burner nozzle along with nitrogen gas as a carrier gas. The TTIP vapour was combined with oxygen gas (an oxidizer) and methane gas (a fuel) in a burner and the mixture heated to combustion. The resultant TiO₂ nanoparticles loaded in the flowing product gas were transported to the collection chamber and separated from the product gas by filtration through a High Airflow Particulate Air (HAPA) filter. The obtained TiO₂ nanopowder (hereafter referred to as the as-received TiO₂ nanopowder) was heat treated at 400, 500, 600, 700, 800 or 900 °C for 1 h in air. Hereafter, the heat-treated powders are referred to as HTxxx, where xxx indicates the treatment temperature in degrees Celsius.

2.2. Characterization of crystalline and electronic structures

The as-received and heat-treated TiO₂ nanopowders were characterized using X-ray diffraction for determining the constituent

* Corresponding author. Fax: +82 2 958 5529.

E-mail address: jkpark@kist.re.kr (J.-K. Park).

phase(s) and particle size (XRD; Bruker D8 Advance) [17], and transmission electron microscopy for determining the shape and size of the particles (TEM; FEI Technai G²).

The hole structures in the conduction band of the TiO₂ nanopowders were directly investigated under UV irradiation by NEXAFS (Near-Edge X-ray Absorption Fine Structure; 7B1 KIST B/L at the Pohang Accelerating Laboratory (PAL), Korea). The powder samples were compacted into thin disks without using any polymer binder in order to prevent surface charging and additional effects associated with polymer binders. Two kinds of 8 W UV-lamps, radiating UVA ($\lambda = 320\text{--}400\text{ nm}$) and UVB ($\lambda = 280\text{--}320\text{ nm}$), were installed together in the NEXAFS chamber. The compacted disk was mounted on the specimen holder and positioned vertically beneath the UV lamp. The UV lamp was located 50 cm from the substrate surface, forming an angle of 15° from the normal. Prior to data acquisition, the NEXAFS chamber was evacuated to 10⁻⁹ Torr. The incident beam was irradiated perpendicular to the substrate

surface and the resultant photo-current was recorded. The respective O K and Ti L edge spectra were recorded for every sample under normal NEXAFS conditions prior to turning on the UV lamp. Additional O K and Ti L edge spectra were obtained twice for every sample under sequential irradiation with UVA followed by UVB. These NEXAFS spectra are referred to as 'UVA1 and UVA2' and 'UVB1 and UVB2'. Just after turning off the UVB lamp, two additional scans of the compacted disk (called OFF1 and OFF2) were performed.

2.3. Measurements of photocatalytic activities

The photoreactivity of the TiO₂ nanopowders was determined from the reaction rates of the oxidative degradation of 2-propanol into CO₂ and water on the surface of the TiO₂ photocatalysts under UV light irradiation in the presence of water and oxygen. Briefly, 50 mg of the TiO₂ nanopowder was suspended in a quartz cell

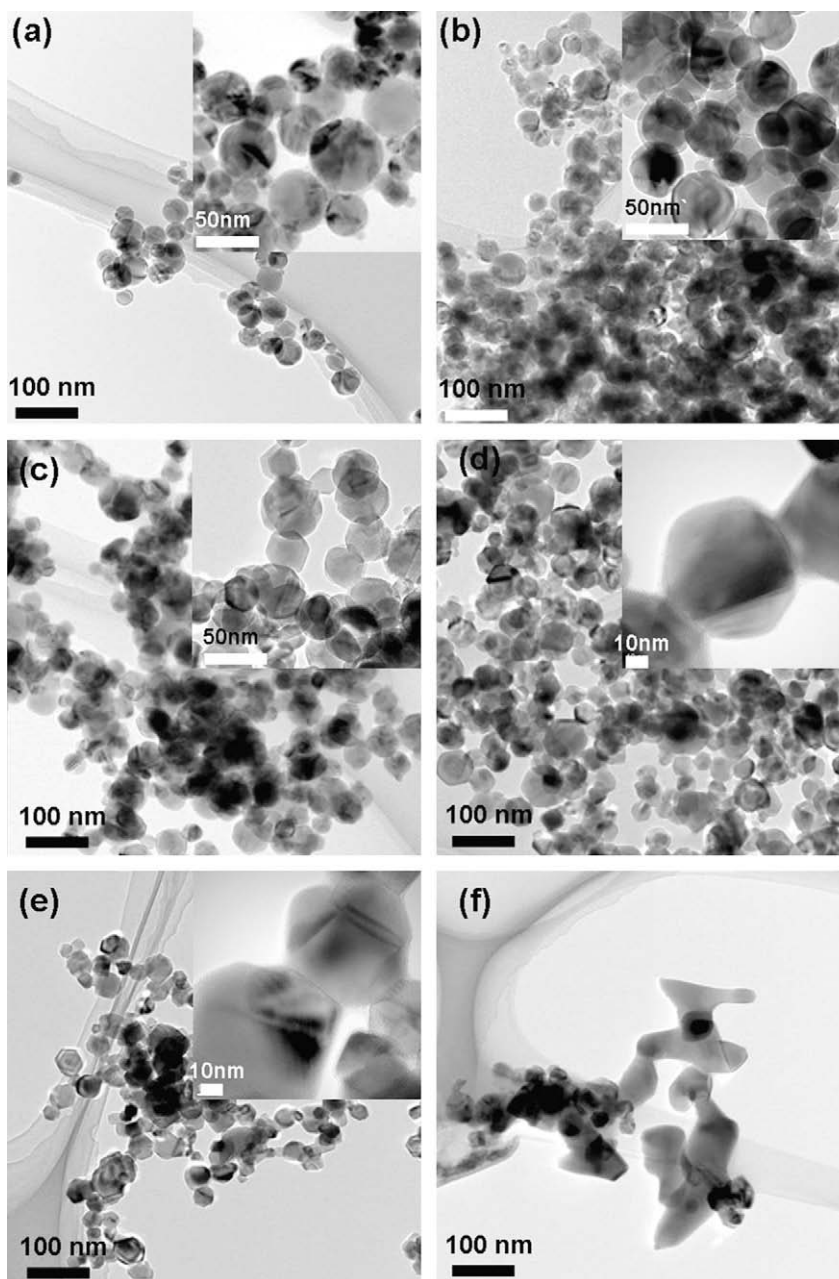


Fig. 1. TEM images of TiO₂ nanopowders: (a) as-synthesized, (b) HT500, (c) HT600, (d) HT700, (e) HT800 and (f) HT900.

containing an aqueous solution of 2-propanol (2.6×10^{-3} mol dm $^{-3}$, 25 mL). Prior to UV light irradiation, the suspension was stirred for 30 min under an oxygen atmosphere in the dark. Then, at 295 K, the suspension was continuously stirred under an oxygen atmosphere and simultaneously irradiated with UV light

($\lambda > 254$ nm) emitted from a 100 W high-pressure Hg lamp. Aliquots (2 mL) taken from the solution at regular intervals were centrifuged and filtered through a Millipore filter to separate the TiO $_2$ particles from the solution, and then analyzed by gas chromatography.

3. Results and discussion

3.1. Catalyst characterization

The as-received and heat-treated TiO $_2$ nanopowders were observed with TEM and their respective images are shown in Fig. 1. The particles of the as-received TiO $_2$ nanopowder are spherical in shape. These spherical TiO $_2$ particles were found to change into a euhedral shape at 500 °C (Fig. 1c), and then to octagonal and cuboidal shapes after heat treatment at temperatures of 600 °C and above (Fig. 1d–f). The inset of each image shows the detailed morphologies of the TiO $_2$ particles under high magnification. Inter-particle necking is evident above 700 °C.

From the XRD patterns of TiO $_2$ nanopowders, the average crystallite size of anatase and rutile and the ratio between two phases shown in Fig. 2 [15]. The as-received powder was almost anatase phase containing about 2% of rutile phase. An anatase-to-rutile phase transition occurred above 700 °C and was completed at 900 °C. The content of rutile phase TiO $_2$ increased to 5% at 700 °C, 23% at 800 °C, and finally 99% at 900 °C in the powder. From the X-ray diffraction data, the anatase-phase TiO $_2$ particles were estimated to grow slightly from 50 nm to 55 nm in diameter with heat treatment up to 700 °C. On the other hand, the diameter of rutile-phase TiO $_2$ particles in the HT800 powder was estimated to about 55 nm, very close to that of anatase-phase particles. Therefore, the morphology change of anatase-phase TiO $_2$ particles below 700 °C is believed not to have a direct relation with the phase transition, but to be related to surface relaxation through surface diffusion with help of enhanced atom mobility, because there is neither anatase-to-rutile phase transition nor evident particle coarsening.

3.2. Evaluation of photocatalytic activity

Fig. 3 shows the results of the photocatalytic degradation of 2-propanol with the as-received and heat-treated TiO $_2$ nanopowders. The degradation rate of 2-propanol increased with increasing heat-treatment temperature up to 800 °C. Interestingly, the degradation rate increased continuously up to 700 °C, despite no evident differences in the phases of the TiO $_2$ nanopowder particles

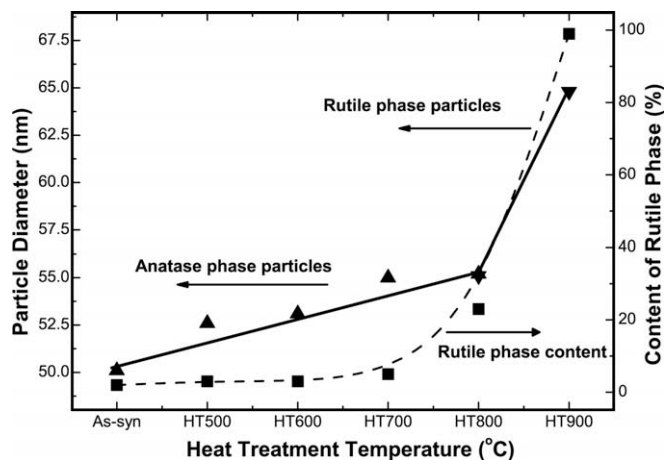


Fig. 2. Variations of TiO $_2$ particle size and content of rutile phase in the powders with heat treatment.

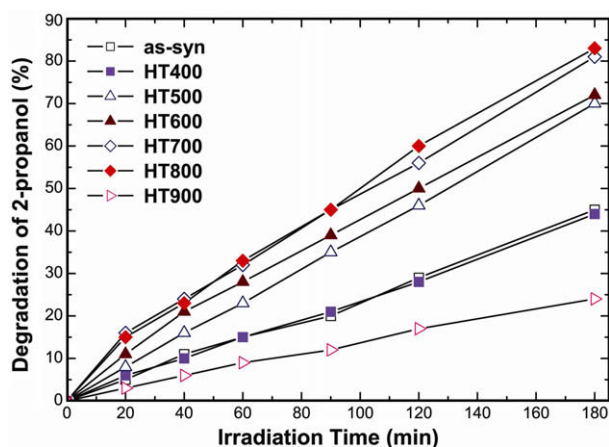


Fig. 3. Photocatalytic degradation of 2-propanol under UV irradiation by various kinds of TiO $_2$ nanopowders (as-synthesized and heat-treated).

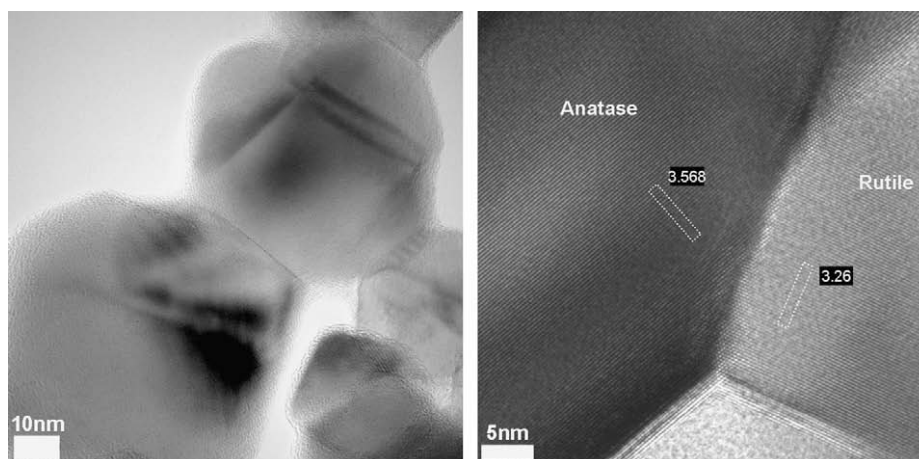


Fig. 4. TEM images showing the anatase–rutile phase boundary in the TiO $_2$ nanopowder treated at 800 °C.

treated with temperatures up to 700 °C, as shown in Fig. 2. Improvement in the photocatalytic property of TiO₂ nanopowders with heat treatment up to 700 °C seems to be correlated to the change of particle shape. Further improvement in the photocatalytic property of HT800 is attributed to the contribution of the anatase/rutile phase boundary [16,17], which was accompanied by the anatase-to-rutile transition, as shown in Fig. 2. Over 800 °C, the degradation rate of 2-propanol decreased drastically, due to the presence of a large fraction of rutile phase with poor photocatalytic activity [18].

Various factors potentially contribute to the considerable improvement in the photocatalytic activity afforded by heat treatment with temperatures of up to 700 °C. Changes in the internal phase and particle size may affect the photocatalytic activity, but Figs. 1 and 2 show that both the internal phase change and particle coarsening are negligible during heat treatment up to 700 °C. However, the TEM images show that the spherical morphology of the as-prepared TiO₂ particles changes to a euhedral shape following

heat treatment at 500 °C, and then to faceted octagonal and cuboidal shapes after heat treatment at temperatures of 600 °C and above. Thus, the improvement in photocatalytic activity can be attributed to partly faceting of the spherical particles.

In order to identify the existence of anatase–rutile phase boundary in the HT800 powder, several dumbbell-type particles were observed by TEM. Considering both rutile phase content of 23% and almost same size of anatase and rutile phase TiO₂ particles, one rutile phase particle may be statistically estimated to contact with four anatase particles in the HT800 powder. Fig. 4 shows the observation results taken from the HT800 powder dispersed in the ethanol with ultrasonic treatment. Many clear boundaries were found between two particles bonded together. Some of them are anatase–anatase boundaries (grain boundary) and others are anatase–rutile phase boundaries. Low magnification image shows a clear boundary between two particles, which were identified, respectively, as an anatase TiO₂ particle and a rutile TiO₂ particle. It is noteworthy from Fig. 4 that as a result of anatase-to-rutile

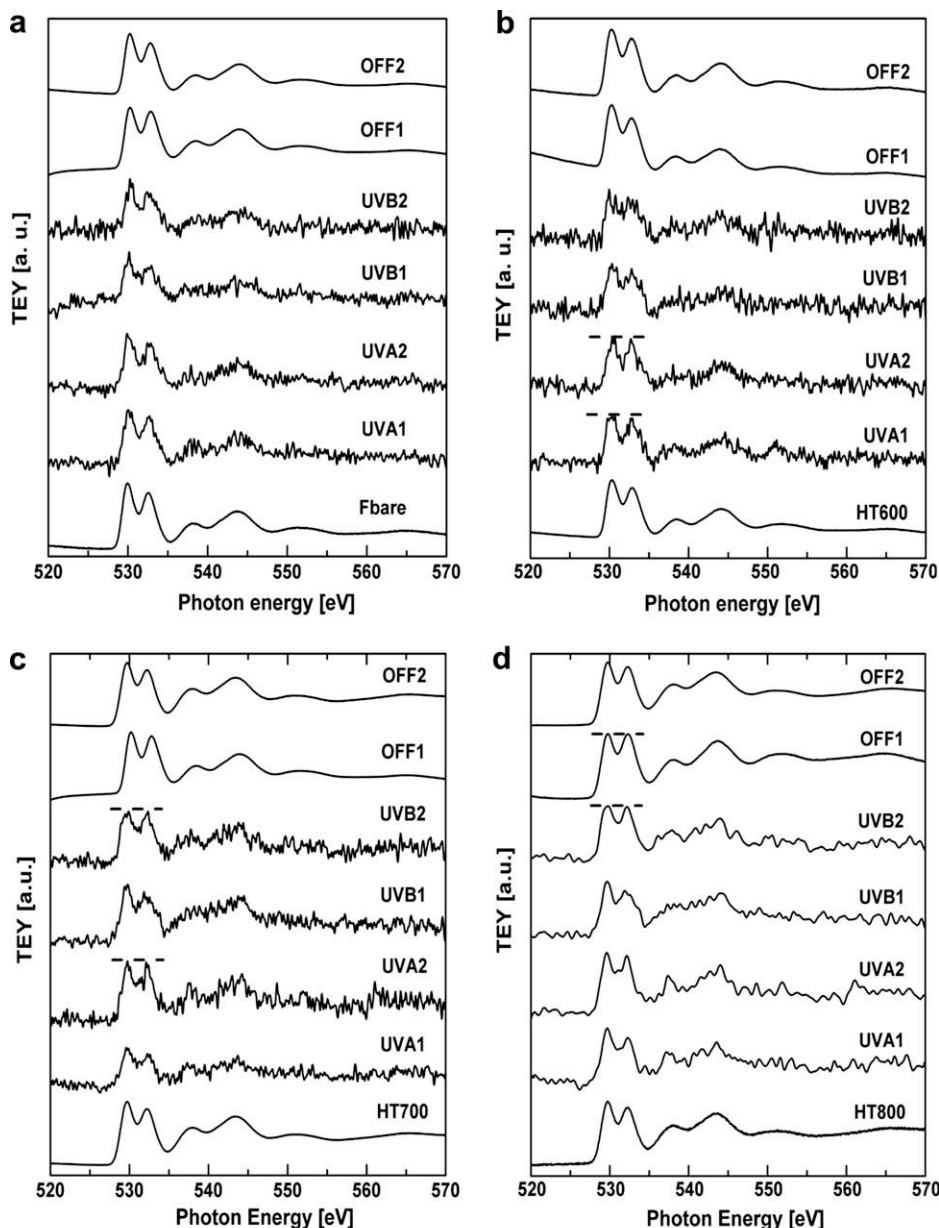


Fig. 5. Variation of oxygen K-edge spectra of TiO₂ nanopowders under UV irradiation: (a) as-synthesized, (b) HT600, (c) HT700 and (d) HT800.

phase transition, an anatase–rutile phase boundary, strong enough not to be broken easily during dispersion, is formed, which can play an important role on the photoreactivity of TiO₂ nanopowders in the present study.

3.3. Determination of hole structure under UV irradiation

The photocatalytic behavior of the TiO₂ nanopowders is closely related to their electronic structures, especially the hole structures of the TiO₂ nanopowders, because the photo-excited electrons from the valance band fill the holes in the conduction band leaving holes in the valance band, and both the photo-excited electrons in the conduction band and the resultant holes in the valance band play a key role in the photocatalytic reaction. NEXAFS is known to be an adequate method for determining the hole structures in conduction bands. In general, the holes in the conduction band are filled with electrons excited from the valance band, according to the excitation energy determined by the wavelength of incident light, which leads to a decrease in the intensity of the holes with correspondent energy. Fig. 5 shows the in-situ NEXAFS observation of the O K-edge spectra of the photocatalysts under UV irradiation. Fig. 5a shows a hole structure in the conduction band of the as-received TiO₂ nanopowder, which was well matched with that of TiO₂ with the anatase form. Interestingly, when the samples were irradiated with UV light, serrated curves were obtained irrespective of the sample condition. However, when the UV light was turned off, the serrated curves returned to their original smooth profile.

We determined the peak position, as well as the variation of relative peak area between the t_{2g} and e_g levels, as a function of heat-treatment temperature. In order to determine both relative peak area and peak position of t_{2g} and e_g in each condition, the NEXAFS curves in Fig. 5 were deconvoluted, respectively, to separate the t_{2g} and e_g peaks. Comparing with the t_{2g} and e_g peaks obtained from the as-received and HT600 powders, those obtained from HT700 and HT800 powders tend to move simultaneously to the low energy side, 0.8 eV for t_{2g} and 0.4 eV for e_g . In addition, in spite of relatively greater shift of the t_{2g} peak against e_g , it was found that the e_g peak broadened and its tail of low energy side expanded towards t_{2g} peak area below the peak intensity energy position of t_{2g} by 0.4 eV approximately. For comparison, the low energy minima of e_g peak of as-received and HT600 powders were found almost same with the peak intensity energy position of t_{2g} within the error limit. Each area of t_{2g} and e_g peaks was calculated and the relative peak area of $[A_{t_{2g}}/A_{e_g}]$ between t_{2g} and e_g was determined. The as-received and HT600 nanopowders showed almost no change in the $[A_{t_{2g}}/A_{e_g}]$ by about 0.77 during UVA1 irradiation while the HT700 and HT800 nanopowders showed large values of $[A_{t_{2g}}/A_{e_g}]$, 1.52 and 1.30, respectively, which means that the peak area of e_g decreased significantly compared with that of t_{2g} . In other words, the holes in the e_g level were filled predominantly with electrons excited from the valance band under UVA1 irradiation. During subsequent irradiation from UVA2 to UVB2, the $[A_{t_{2g}}/A_{e_g}]$ values were kept around 0.70 slightly lower than that of unexposed nanopowder (0.77) and maintained even after turning off UVB(OFF1), meaning that the holes in the t_{2g} level were filled relatively more than those in the e_g level. Then, the $[A_{t_{2g}}/A_{e_g}]$ value was recovered to that of unexposed powder at OFF2.

Present analyses of t_{2g} and e_g peaks show that the conduction band of TiO₂ nanopowders synthesized in the present study moved to the low energy side with heat treatment at the elevated temperature above 700, which leads to easy excitation of valance electrons and subsequent decrease in hole density at the t_{2g} level. The electrons filling the t_{2g} level resided in the conduction band as long as about 30 min after turning off UV irradiation. Another

interesting finding in the present analysis was the preferential filling of holes in the e_g level in the HT700 and HT800 powders. Even though the preferential filling of e_g level seems to be related to the broadening of e_g peak of which tail in the low energy side is extended toward t_{2g} peak, the variation of the hole structures with heat treatment at elevated temperature should be verified further.

The change in the hole structures of the TiO₂ nanopowders seems to correspond well with the change in their photocatalytic properties shown in Fig. 3, which was determined under UV light irradiation with wavelengths longer than 254 nm. As the lifetime of the excited electrons in the conduction band increased, the photoreactivity of the TiO₂ nanopowders improved. The relationship between Figs. 3 and 5 can be explained in terms of microstructural aspects, specifically, in terms of the existence of an anatase/rutile phase boundary, which is known to act as a cationic trap for electrons excited from the valance band [19,20]. The as-received TiO₂ nanopowder contained about 10% rutile phase, which remained almost intact below about 700 °C. The anatase-to-rutile phase transition proceeded rapidly above 800 °C, and was almost completed at 900 °C. With the help of surface diffusion causing nonfaceted–faceted transitions in the particle shape in Fig. 1, the necks at the particle contacts grow with heat treatment; direct evidence of this is found in the observation of neck growth between the TiO₂ particles in Fig. 1. Similarly, contact areas between anatase and rutile particles form anatase/rutile phase boundaries that increase in size as the heat-treatment temperature is increased, even at temperatures below 700 °C. The anatase phase transforms to the rutile phase at a fast rate above 800 °C, and the anatase/rutile phase boundary disappears at 900 °C. This change in the anatase-to-rutile phase boundary corresponds well with the gradual improvement in the photocatalytic properties in accordance with the heat-treatment temperature. As the area of the anatase/rutile phase boundary increased, more electrons became trapped in the phase boundary because upward distortion of the conduction band in the space charge layer of anatase crystal in contact with rutile crystal blocks the electron transfer from anatase to rutile crystal, resulting in a long lifetime in the conduction band [20,21].

The present findings give direct experimental evidence showing, for the first time, that the electrons trapped in the anatase/rutile grain boundary suppress the recombination of electrons and holes, and in turn, this suppression of recombination contributes directly to the improvement in the photocatalytic property of flame-synthesized TiO₂ nanopowders.

4. Conclusions

The anatase-phase-rich TiO₂ nanopowders containing very small volume fraction of rutile phase were fabricated by the flame method and treated at elevated temperatures to improve their photoreactivity. Their photoreactivity increased with increasing heat-treatment temperature within the limit of the anatase-phase-rich condition, but decreased drastically with formation of the rutile phase as a result of the anatase-to-rutile phase transition. The hole structures in the conduction band of TiO₂ nanopowders were directly determined by in-situ NEXAFS measurements under UV light irradiation. The NEXAFS results showed that the photoexcitation of electrons from the valance band became more evident as the heat-treatment temperature increased up to 800 °C. The improvement in photoreactivity of the TiO₂ nanopowders is attributed to both the change of particle shape at the low temperature region and the existence of an anatase/rutile phase boundary, which traps excited electrons and suppresses the recombination of electrons and holes, causing the photo-induced electrons to have long lifetimes.

Acknowledgments

The NEXAFS measurements at PLS were supported in part by MOST and POSTECH.

References

- [1] C.H. Cho, M.H. Han, D.H. Kim, D.K. Kim, *Mater. Chem. Phys.* 92 (2005) 104.
- [2] T. Ohno, K. Sarukawa, M. Matsumura, *J. Phys. Chem. B* 105 (2001) 2417.
- [3] K. Nakaso, K. Okuyama, M. Shimada, S. Pratsinis, *Chem. Eng. Sci.* 58 (2003) 3327.
- [4] S.U. Khan, M.U.M. Al-Shahry, W.B. Ingler Jr., *Science* 297 (2002) 2243.
- [5] B. Neppolian, H.S. Jie, J.P. Ahn, J.K. Park, M. Anpo, *Chem. Lett.* 33 (2004) 1562.
- [6] H. Park, B. Neppolian, H.S. Jie, J.P. Ahn, J.K. Park, M. Anpo, D.Y. Lee, *Curr. Appl. Phys.* 7 (2007) 118.
- [7] C.B. Almquist, P. Biswas, *J. Catal.* 212 (2002) 145.
- [8] J.-H. Lee, Y.-S. Yang, *Mater. Chem. Phys.* 93 (2005) 237.
- [9] H. Wang, Y. Wu, B.-Q. Xu, *Appl. Catal. B: Environ.* 59 (2005) 139.
- [10] C.K. Chan, J.F. Porter, Y.-G. Li, W. Guo, C.-H. Chan, *J. Am. Ceram. Soc.* 82 (1999) 566.
- [11] C.H. Cho, D.K. Kim, D.H. Kim, *J. Am. Ceram. Soc.* 86 (2003) 1138.
- [12] J.F. Porter, Y. Li, C.K. Chan, *J. Mater. Sci.* 34 (1999) 1523.
- [13] T. Taguchi, Y. Saito, K. Sarukawa, T. Ohno, M. Matsumura, *New J. Chem.* 27 (2003) 1304.
- [14] S. Yang, L. Gao, *J. Am. Ceram. Soc.* 88 (2005) 968.
- [15] R.A. Spurr, H. Myers, *Anal. Chem. Res.* 29 (1957) 760.
- [16] T. Miyagi, M. Kamei, T. Mitsuhashi, T. Ishigaki, A. Yamazaki, *Chem. Phys. Lett.* 390 (2004) 399.
- [17] D.C. Hurum, A.G. Agrios, K.A. Gray, T. Rajh, C. Thurnauer, *J. Phys. Chem. B* 107 (2003) 4545.
- [18] Yu.V. Kolen, B.R. Churagulov, M. Kunst, L. Mazerolles, C. Colbeau-Justin, *Appl. Catal. B: Environ.* 52 (2004) 51.
- [19] G.S. Herman, Z. Dohnalek, N. Ruzycski, U. Diebold, *J. Phys. Chem. B* 107 (2003) 2788.
- [20] Bo Sun, Panagiotis G. Smirniotis, *Catal. Today* 88 (2003) 49.
- [21] Bo Sun, Alexandre V. Vorontsov, Panagiotis G. Smirniotis, *Lanmuir* 19 (2003) 3151.